# *CHAPTER 6*

## *A. Unusual Double Glassy phase and Anomalous Hall effect in S-doped $(SbFe)_2Te_3$ Topological Insulator*

### 6.A.1 Introduction:

Topological insulators (TIs) belonging to the new class of quantum matter possess insulating bulk and linearly dispersed conducting surface states protected by time reversal symmetry (TRS)[15], [17], [293], [294]. The unique electronic states, known as topological surface states (TSS) exhibit chiral spin arrangements and originate from the inversion of bulk bands as a result of strong spin-orbit coupling. The electrical transport is robust against backscattering of nonmagnetic perturbations on the spin- momentum locked surface states. This exotic Dirac surface states are attractive for various electronic applications and potentially host a range of intriguing phenomena including the quantum spin Hall effect, the topological magnetoelectric effect, quantum anomalous Hall effect, and Majorana fermions[15], [294]–[297]. In order to determine the optimal set of dopants, magnetic order, and transport properties, impurity induced TI has taken intensive research interests among the condensed matter family. The ferromagnetic, antiferromagnetic, and spin frustration on the surface of a 3D TI are only a few examples of the diverse spin configurations that come from the interaction between the RKKY interaction and the geometry of the spin lattice. [298]–[301]. Although, many works were dedicated to incorporate magnetism through surface/bulk doping for the potential diluted magnetic semiconductors (DMS), very few letters are reported where SG/CG phase has been observed in TI. Moreover, there are many reports that are particularly dealing with Fe doping, such as Fe doped $Bi_2Te_3$ [302]–[305], Fe doped $Sb_2Te_3$ [111], [306]–[308], Fe doped $Bi_2Se_3$ [309]–[311], but observation of such unusual phase called glasy phase is very scarce. Indication of spin glass/cluster glass state were found in the works on Mn doped $Bi_2Se_3$ and Fe intercalated $Bi_2Te_3$[69], [301]. But previous studies on magnetism of impurity induced $Bi_2Te_3$ and $Sb_2Te_3$ were limited to DC magntization measurements, performing ac suceptibility measurements with an aim of direct observation of SG/CG

phase is missing in this family of compound. To the best of our knowlegde the detail magnetic study on glassy phase among TI family is yet to be performed. Interestingly, we found room temperature ordering in $Fe_{0.1}Sb_{1.9}S_{0.15}Te_{2.85}$ compounds, such higher ordering is again very uncommon among paramagnetic TI family ($Sb_2Te_3$, $Bi_2Te_3$, $Bi_2Se_3$) with induced magnetic dopants. So, the pertinent question that arises related to such system like what is the ground state and does long range ordering exists in this impurity induced paramagnetic TI system and if exists does it coexist with SG phase, is scientifically investigated and logically comprehended in this thesis.

In this work, we investigated the unusual spin orders on topological insulators $Sb_{1.9}Fe_{0.1}Te_{2.85}S_{0.15}$ in a quest for an exclusive platform that can host both magnetic fluctuations and Dirac quasiparticles at the same time. The dc magnetization along with the ac susceptibility data render the system a cluster SG type at low temperature due to the competive FM-AFM interactions present in the system. Within our knowledge scope, so far, the glassy phase has not been reported for $Sb_2Te_3$. We also present evidence for a Griffith like phase (GP) at low field in $Fe_{0.1}Bi_{1.9}Te_3$ similar to [301] and described in chapter 6.B. Topological frustrated magnetic sublattices, particularly when combined with relativistic carriers, are uncommon, and investigation of their Hall effects has been sparsely performed. The dHvA oscillation consists of three frequencies, and the corresponding Fermi surfaces (FSs) are identified to be originating from nontrivial bandstructure.

### 6.A.2 Results and Discussions

**6.A.2.1 XRD** Naturally, single crystals prefer to cleave along the [001] direction, resulting in the normal direction of these flakes being (001), The strong (00l) (l = 6, 9, 12, 15, 18) diffraction peaks Figure 6.A.1a indicate that the single crystal is c-oriented crystal flake. The crystals were confirmed to be single phase without any impurity and secondary phases

and identified as having rhombohedral R-3m (space group=166) crystal structure by x-ray diffraction.

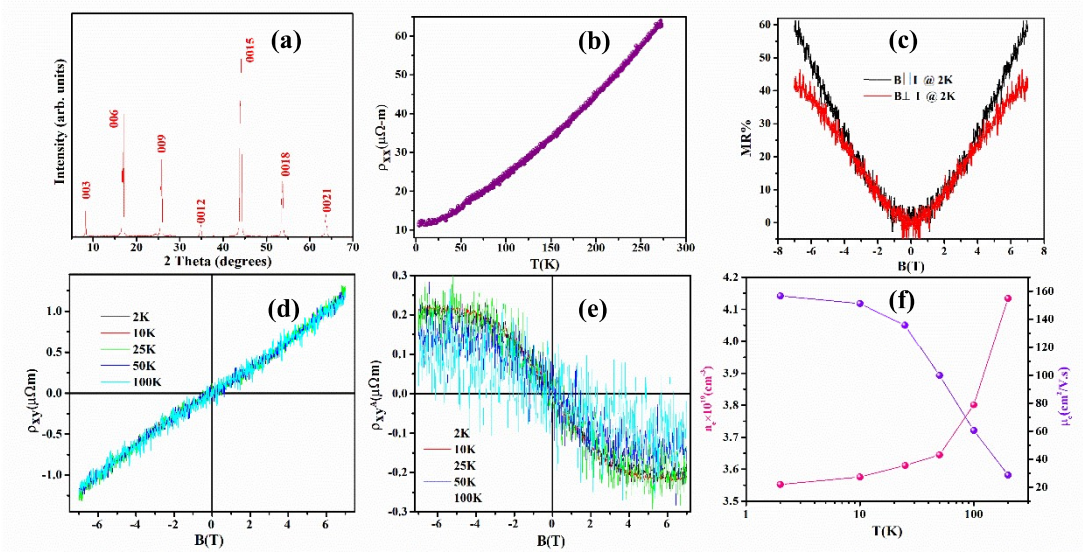


**Figure 6.A.1 (a)** Single crystal XRD pattern of $Sb_{1.9}Fe_{0.1}S_{0.15}Te_{2.85}$, **(b)**resistivity evolution with temperature at zero magnetic field, **(c)**MR% at 2K for B∥I and B⊥I configuration, **(d)** Hall resistivity at 2K, 10K, 25K, 50K and 100K, **(e)** AHE effect at 2K, 10K, 25K, 50K and 100K, **(f)** density and mobility evolution with temperature.

$Sb_{1.9}Fe_{0.1}S_{0.15}Te_{2.85}$ has the same crystal structure with the R-3m compounds, with lattice parameters of a = b = 4.269 Å, c = 30.499 Å. The crystal growth direction is parallel to the ab plane, as seen in Figure 6.A.1a. All of the peaks can be identified as (00l) reflections, as labelled on the pattern, heralding the cleaved surface is in c direction only. Powder XRD was further confirmed the phase of the samples.

**6.A.2.2 Resistivity behaviour** As shown in the temperature dependence of the resistivity in Figure 6.A.1b, ρxx has a residual resistivity ratios (RRR) = R(300 K)/R(2 K) of more than 5.21, lower RRR value implies higher impurity scattering. This value is compatible with a number of topological materials. The magnetic field dependency of the MR is illustrated in Figures 6.A.1c, with two different measurement geometries. The resulting MR ratio $\Delta MR \equiv [\rho_{xx}(7\ T) - \rho_{xx}(0\ T)]/\rho_{xx}(0\ T)$ reaches 60%, 40.78% at 2K for B|| I and B⊥I.

To explore detailed information about the transport process, we performed the Hall effect measurements. Figure 6.A.1d presents the Hall resistivity $\rho_{xy}$ as a function of magnetic field at various temperatures. The positive slope of $\rho_{xy}$ indicates that the dominant charge carriers are holes. We then obtain the anomalous Hall component by subtracting the ordinary Hall component. The resulting $\rho^{AHE}_{xy}$ is shown in Figure 6.A.1e. The carrier concentration becomes n =2.3 ×1020 $cm^{-3}$ and a mobility of 3800 $cm^2$ /V.s at lowest temperature as estimated from the low-field slope (Figure 6.A.1f). In a ferromagnet, $\rho_H$ is defined as $\rho_H = \rho^0_H + \rho^A_H = R_0B + R_s\mu_0M$, where $\rho^0_H$ ($\rho^A_H$ ) and $R_0(R_s)$ are the ordinary (anomalous) Hall resistivity and coefficient, respectively. Other than the ordinary Hall effect produced by Lorentz force, the additional term is an anomalous term which is proportional to the spontaneous magnetization M. The microscopic origin of this AHE is (a) intrinsic Berry curvature effects where the anomalous Hall conductivity $\sigma^A_{xy}$ scales quadratically with longitudinal resistivity $\sigma_{xx}$ ($\sigma^A_{xy} \propto \sigma^2_{xx}$) and (b) extrinsic effects like skew scattering ($\sigma^A_{xy} \propto \sigma_{xx}$) and side-jump ($\sigma^A_{xy} \propto \sigma^2_{xx}$). Presently, the frustrated structures, noncollinear magnetism, some spin-ice and spin-liquid state has proved to be the topic of significant interest in the AHE research[86], [90], [264], [312]–[316]. The present system follows the proposed “spin cluster” mechanism by Ishizuka and Nagaosa [87]. When an external field causes a distortion of the local order, magnetic fluctuations act as scattering centres, providing an enhanced skew scattering potential. A large spin Hall angle is produced by this spin-cluster scattering, which is the case of our present investigation. The Hall angle is $\sigma^{(AHE)}_{xy}/\sigma_{xx}$ ~0.063, comparatively larger than the conventional limit of AHA~ $10^{-3}$–$10^{-2}$[317]. However, the AH conductivity and transverse conductivity are not that large ($\sigma^A_{xy}$~101.3$\Omega^{-1}cm^{-1}$ , $\sigma_{xx}$~ 909.5$\Omega^{-1}cm^{-1}$ at 2K) as specified in enhanced skew scattering cases produced by multi spin/tilted spin-cluster/geometrically frusted lattice[86], [266], [316].

**6.A.2.3 Magnetic behaviour** In order to explore the magnetic behavior of the $Sb_{1.9}Fe_{0.1}S_{0.15}Te_{2.85}$ single crystal, the temperature dependence of zero field cooled-field warm (ZFC-FW) and field cooled-field warm (FC-FW) magnetization with an external field of 100,1000 and 4000 Oe was recorded in the temperature range 2-350K and is shown in (a) of Figure 6.A.2. The 100 Oe ZFC-FC data is shown separately in Figure 6.A.2b.

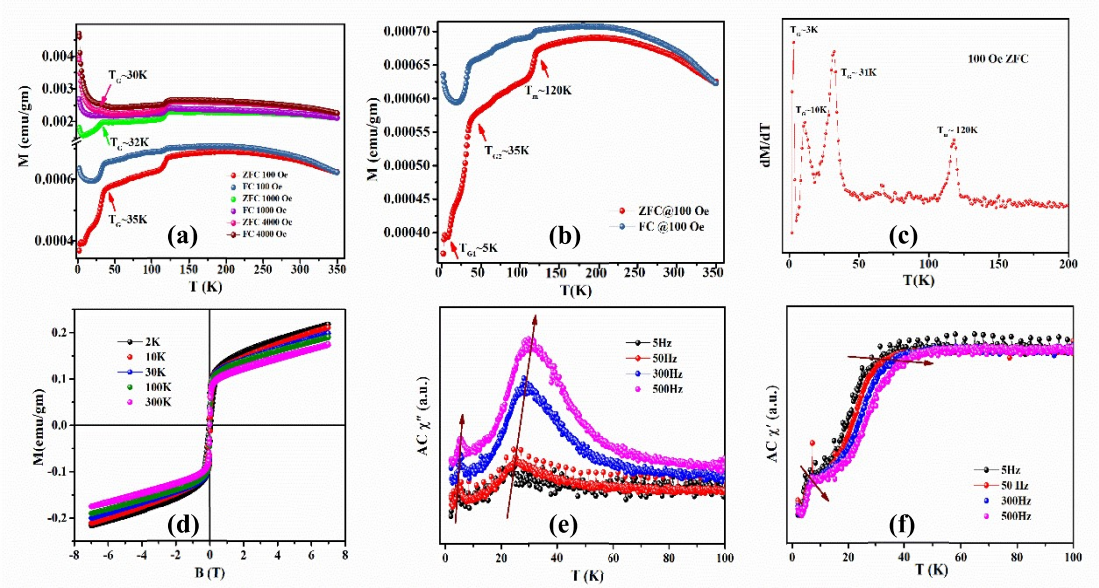


**Figure 6.A.2 (a)** dc magnetization vs temperature for $Sb_{1.9}Fe_{0.1}S_{0.15}Te_{2.85}$ measured between 2 and 350 K at 100 Oe, 0.1T, and 0.4T, **(b)** ZFC and FC curves for 100 Oe, **(c)** dM/dT for 100 Oe ZFC curve to obtain the transition temperatures from inflection points, **(d)** Field dependence of magnetization measured at different temperatures, Temperature dependence of the **(e)** real ($\chi'$) and **(f)** imaginary ($\chi''$) components of the ac susceptibility measured at frequencies varying from 5 to 500 Hz.

Below room temperature, the ZFC & FC M(T) data clearly reveals three anomalies near 112, 31 and 4K. In addition, the ZFC and FC M(T) curves show bifurcation due to history dependent effects. Such bifurcation has been reported in spin-glass and superparamagnetic (SPM) systems [1–5]. In canonical spin glasses, ZFC M(T) shows a cusp at $T_{max}$ and the bifurcation of FC and ZFC M(T) occurs close to the cusp temperature [1–4]. Most importantly, the peaks around ~4K and 31K in M(T) of this system is quite sharp. We can observe pronounced peak near 125K, this magnetic transition is also observed in Fe doped

$Sb_2Te_3$, this transition was due to change in average magnetic interactions from FM to AFM in Fe intercated $Bi_2Te_3$ system [38]. They found a clear deviation or hump near about T=120K for x=0.025. However, our isostructural compound Fe doped $Sb_2Te_3$ shows similar type of increasing trend in magnetic moment near 120K from M-T data. This increase in M-T is a probable indication of quantum Griffith phase below paramagnetic region similar to [38]. We can see clear ordering upto 350K, no signature of AFM to paramagnetic transition we can observe up to this temperature for $Fe_{0.1}Sb_{1.9}S_{0.15}Te_{2.85}$ system. So, we cannot comment about Neel temperature at this moment. However, we can also observe a sharp drop in moment with increasing temperature for this compound. The drop is more prominent in 100Oe ZFC FC data compared to the higher fields. This type of long-range AFM ordering with glassy phase at lower temperature was also reported in [18]. The nature of ZFC M(T) response of this compound is, however, is like a typical AFM transition because the magnetic moment is continuously increasing up to 120K, then saturates and finally starts to decrease above 350K from the Figure 6.A.2b.

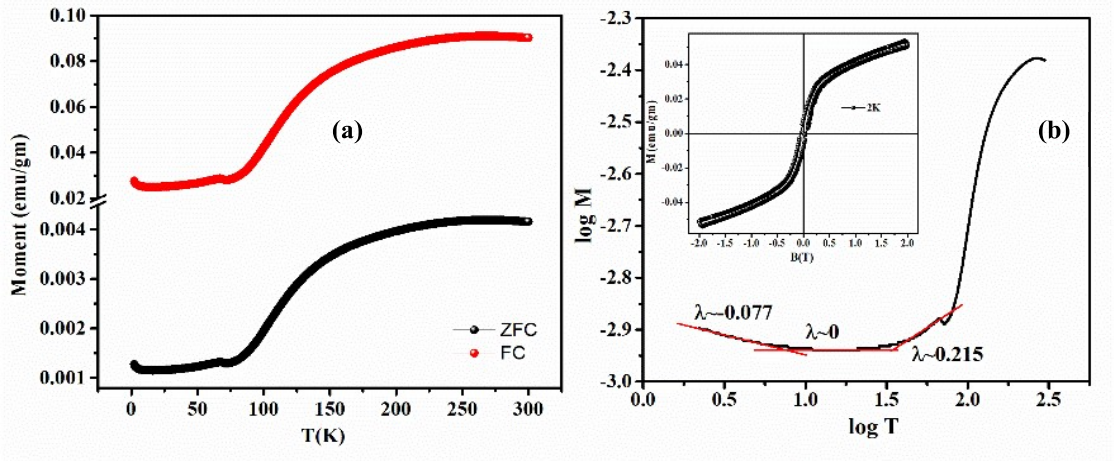


**Figure 6.A.3 (a)** The ZFC and FC susceptibilities vs T measured at H = 0.1 T, **(b)** the log-log plot of the M(T) curve along with the linear fits at low temperature**, inset:** evolution of magnetization as a function of field at 2K for $Sb_{1.9}Fe_{0.1}Te_3$.

However, there was no anomaly found below 50K for the Fe doped compound $Sb_2Te_3$ as evidence from 6.A3a. But irreversibility between ZFC FC data (100 Oe) below 250K is an

indication towards glassy systems. Importantly, [38] reported spin freezing behaviour at low temperature as the divergent behaviour of spin susceptibility got saturated at low temperature.

The peak around 125K for $Fe_{0.1}Sb_{1.9}S_{0.15}Te_{2.85}$, however, starts getting smeared out at low field and the bifurcation starts well above $T_{max}$~350K unlike canonical SG systems. Observation of such smeared peaks have been reported in several cluster glass and SPM systems due to occurrence of freezing/blocking over a wide range of temperatures as a result of large distribution of cluster sizes [6-8].

The irreversibility below 345 K between FC curve and ZFC curve is clear with applied field of 100 Oe and 1 KOe but it is about to supress in higher field above 4 kOe. The ZFC and FC curves show a maximum at $T_{m1}$=35K and $T_{m2}$=122K respectively. The decrease of ZFC magnetization below $T_{m1}$ is due to the random freezing of the clusters into different metastable states [9,10]. At low field FC magnetization decreases with deceasing temperature, this behaviour is common among cluster spin glass (CSG) systems with interacting spin clusters. However, increase of field cooled magnetization at higher field (1000 Oe and 4000Oe) below $T_{m1}$ is due to the strong ferromagnetic intercluster interactions. The magnetization is observed to increases with increasing magnetic field. It can be seen that there is no saturation of magnetization curves up to +- 7T suggesting the existence of strong antiferromagnetic intercluster interactions mixed with the ferromagnetic interactions inside the clusters. With increasing the field, the ferromagnetic trends decrease, whereas the antiferromagnetic contribution increases linearly, resulting in lowering of coercivity and saturation magnetization. Figure 6.A.2c illustrates the “dM/dT plot” from which magnetic transitions temperatures can be identified by 4 inflection points at 120K, 31K, 10K and 3K when the dc field is 100Oe. We can see only 2 points from

dM/dT plot when the field increases to 1000 Oe. However, at 4000 Oe, we can see only the long-range magnetic transition temperature. This further demonstrates that the 120K temperature corresponds to an AFM-FM magnetic transition rather than a disordered transition. As the glassy phase destroys with increasing field, we can conclude that the system is a disordered CSG state at low temperature. The nature of ZFC M(T) response of for $Sb_{1.9}Fe_{0.1}S_{0.15}Te_{2.85}$, is like a typical AFM transition as the moment is continuously increasing up to 120K for the ZFC curve. Above 180K, the moment tends to decrease followed by a saturation at about 150K. The paramagnetic transition temperature is not observed up to 350K and the $T_N$ is expected to be quite high.

In the ZFC run along the easy direction, low applied fields can easily direct these random spins (or domains) to flip along its direction in a parallel FM-like manner. In that case, the net magnetic moment gained, increases with temperature up to the peaks position. At higher temperatures, the second antiparallel exchange coupling state is more favoured and an AFM-like structure (with much smaller net moments) is obtained. This is similar to [11] which describes the ZFC and FC nature of the saturated isothermal remanent magnetization of this material. With time under ambient conditions, the unstable AFM-like state switches back to its random ground state as shown in Figure 6.A.2b.

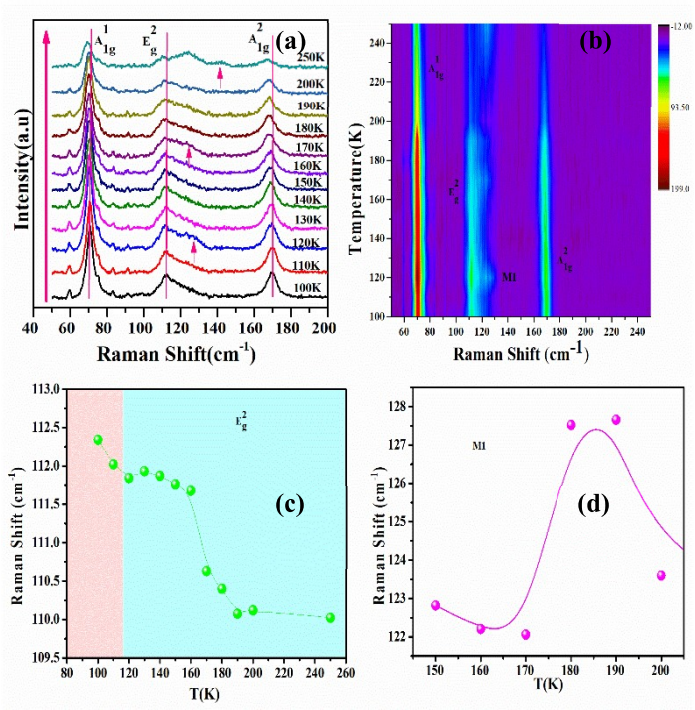


**Figure 6.A.4** Temperature dependent **(a)** Raman spectra, **(b)** 3D plot to see the clear variation between different modes, **(c)**Temperature evolution of the Raman shift of the $E_g$ mode, and **(d)** M1 mode of $Sb_{1.9}Fe_{0.1}S_{0.15}Te_{2.85}$.

**6.A.2.4 ac magnetic susceptibility behaviour** The ac magnetic susceptibility measurements $\chi_{ac}(T,f)$ were made in zero dc magnetic field ($H_{dc}$=0) between 2 to 100 K and at the frequency (f) ranging from 5 to 500 Hz using the quantum-squid. Figure 6.A.2e and f presents the real ($\chi'$) and imaginary part ($\chi''$) of ac susceptibility for Fe and S doped $Sb_2Te_3$ as a function of temperature at an ac field of $H_{ac}$ = 5 Oe with several fixed frequencies (f = 5, 50, 300, and 500 Hz). It is found that $\chi''(T)$ (Figure 6.A.2e) exhibits a strong frequency-dependency for the peak around 5K and 25K. As the frequency increases, the peak position shifts towards higher temperatures, while the magnitude increases, suggesting a characteristic feature of typical glassy behavior with a freezing temperature $T_{f1}$= 5K and $T_{f2}$=25K. Although the transition near 5K is not a sharp like 22K and 125K from DC M-T, it is significantly observed in our AC susceptibility data. This transition was not even present in Fe doped $Sb_2Te_3$. We can show that the in-phase part shows a clear

anomaly at 125K which is supposed to be an overall change in magnetic correlation from FM to AFM, although the out-of-phase part shows zero dissipation at this transition, which is an indication of non-glassy magnetic type of transition at this temperature. Although a frequency-dependent shift of $T_f$ is known for both SG freezing and SPM blocking, Mydosh parameter p is the universal tool to distinguish glassy states

$$p = \frac{\Delta T_f}{T_f \Delta log_{10} f} \quad \textbf{(6.A.1)}$$

For typical SPM systems p>0.1, for SG p<0.01 and p value for the CG system lies in between. In the present case, the Mydosh parameter comes out to be 0.098 and 0.072 for $T_{f1}$ and $T_{f2}$ which is basically in the range of cluster glass. However, the p value for the $T_{f1}$ transition is 0.098 which is in the CG range. Our p value for both $T_{f1}$ and $T_{f2}$ is much higher than that of canonical spin glasses (e.g., p = 0.01 [12]) [282], but is two orders of magnitude lower than that of superparamagnets (e.g., p ≈ 3 [12]), and is comparable to values observed for geometrically frustrated magnets [284], [318]. The strength of the interaction between individual spins or magnetic entities influences the freezing temperature dependence on the excitation frequency.

Eventually, the spin dynamics in a glassy state gets slowed down below the critical temperatures $T_f$ which can be investigated using the dynamic scaling law-

$$f = f_0 (\frac{T_f - T_{SG}}{T_{SG}})^{\nu} \quad \textbf{(6.A.2)}$$

where f refers to the frequency for $\chi''$curves attaining a maximum at $T=T_f$, $T_{SG}$ is the equivalent SG freezing temperature with f→0Hz and HDC →0 Oe, and $f_0$ is related to the characteristic spin flipping time ($\tau_0$as $2\pi f = \frac{1}{\tau_0}$); zν is the dynamical critical exponent. The best fitting of the "f vs Tf" curve Figure 6.A.5a, b yielded $f_0=10^5$, $10^6$ Hz; $\tau_0 = 8.54\times10^{-6}$ s, $1.39\times10^{-6}$ s, and $T_{SG}$= 4.05K, 23.032K; zν=3.379 and 3.313 for $Tf_1$ and $Tf_2$ respectively. For conventional SG systems, the value of zν typically lies between ~4 and~12, while the

value of $\tau_0$ ranges from $10^{-12}$ to $10^{-13}$ s [319], [320]. This value of τ0 indicates slow dynamics, as expected for cluster spin glasses, where τ0 is typically in the $10^{-6}$–$10^{-10}$ s range [282], [321]. Our zν value is also comparable with the reported CSG systems [322], [323].

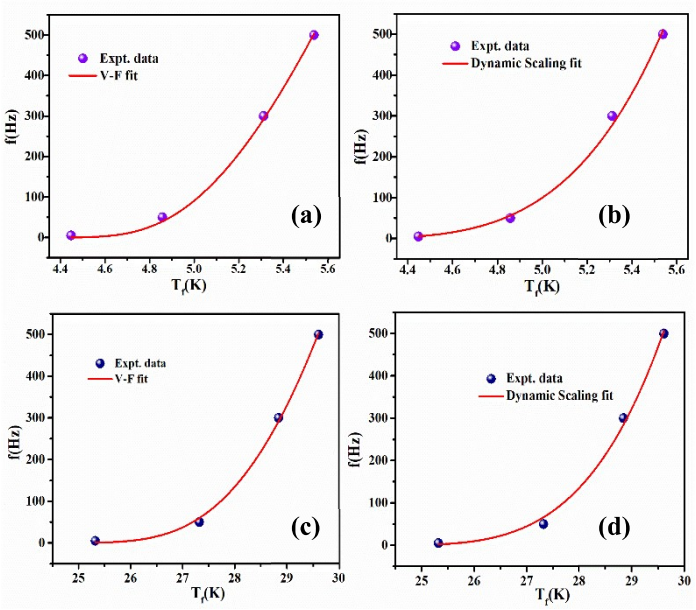


**Figure 6.A.5** Dynamic scaling (a), (b) and Vogel-Fulcher (c), (d) fits of the "$T_f$ vs f" curve respectively for $T_{f1}$ and $T_{f2}$ for $Sb_{1.9}Fe_{0.1}S_{0.15}Te_{2.85}$.

To further investigate intercluster interactions, the empirical Vogel-Fulcher (VF) model [described by Eq. (6)] was employed in fitting the "f vs Tf" curve

$$f = f_0 \, exp\left(\frac{-E_A}{K_B(T_f - T_0)}\right) \qquad \textbf{(6.A.3)}$$

where $T_0$ represents interaction strength between dynamic entities and $E_A$ is the activation energy. The best fit Figure 6.A.5c and d yields $E_A$=0.24meV, 3.64meV; $T_{SG}$= 4.035K, 22.237K for $T_{f1}$ and $T_{f2}$. The $\tau_0$ value obtained from the Vogel–Fulcher fitting for $T_{f1}$ as well as $T_{f2}$ ($\tau_0 = 1.46 \times 10^{-5}s, 3.04 \times 10^{-6}s$) is orders of magnitude larger than the spin-flip time of atomic magnetic moments (~$10^{-13}$ s) and SG systems(~$10^{-11} - 10^{-13}$s). The larger $\tau_0$ indicates toward freezing of magnetic clusters rather than atomic spins. $E_A/K_B$ =

0.397meV, 2.949 meV $T_0$ = 4.035 K, 22.237 K and for $T_{f1}$ and $T_{f2}$. The nonzero $T_0$ arises because of the interaction between the individual spins. It is further denoting that the fluctuating entities are spin clusters with a significant inter-cluster interaction. Moreover, the presence of Ruderman-Kittel-Kasuya-Yosida (RKKY) interaction is indicated by the fact that $T_0$ is near to the freezing temperature $T_f$. According to the Tholence criterion [60]

$$\delta T_{Th} = \frac{T_f - T_0}{T_f} \quad \textbf{(6.A.4)}$$

where $T_f$ is measured at smallest excitation frequency, we extract $\delta T_{Th}$ = 0.089 and 0.039 for $T_{f1}$ and $T_{f2}$. The value of $T_{f1}$ = 4.45 K (for f = 5 Hz), $T_{01}$ = 4.05 K and $T_{f2}$=24.77K (for 5K) and $T_{02}$=23.79K. This value is comparable to other CSG systems [283], [322], [324]. Altogether these analyses suggest that the present system falls in the category of CGS system.

Re-entrant spin glasses (RSG) or cluster spin glasses are systems that exhibit SG properties at temperatures below the ferromagnetic Curie temperature TC [14,15].

**TABLE 6.A.I Parameters obtained from the ac susceptibility analysis using Eqs. (5) for $T_{f1}$ and $T_{f2}$**

| $T_f$(K) | $\tau_0$ (s) | $T_{SG}$(K) | zν |
|---|---|---|---|
| 4.447 for f= 5 Hz | $8.54\times10^{-6}$ | 4.05 | 3.379 |
| 24.77 for f= 5 Hz | $1.39\times10^{-6}$ | 23.79 | 3.313 |

**TABLE 6.A.II. Parameters obtained from the ac susceptibility analysis using Eqs. (6) for $T_{f1}$ and $T_{f2}$**

| $T_f$(K) | $\tau_0$ (s) | $T_0$ (K) | $E_A/K_B$ (K) |
|---|---|---|---|
| 4.447 | $1.46 \times 10^{-5}$ | 4.035 | 4.61 |
| 24.77 | $3.04 \times 10^{-6}$ | 22.237 | 34.25 |

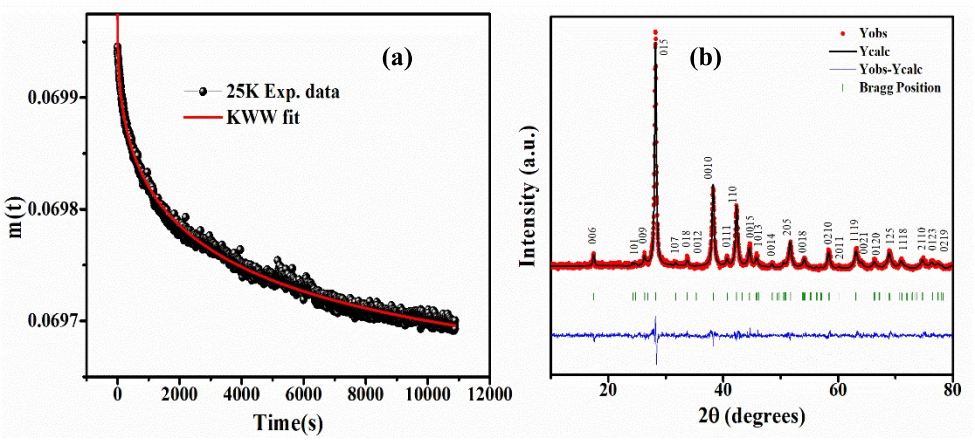


**Figure 6.A.6 (a)** Time dependence of thermoremanent magnetization at 25 K for 0.1T cooling field and wait time of 100s. The solid line is the best fit for KWW function to the data, **(b)** powder XRD pattern and its Rietveld refinement for the sample $Sb_{1.9}Fe_{0.1}S_{0.15}Te_{2.85}$.

Moreover, isothermal temporal relaxation of the remanent magnetization (TRM) at 25K was performed to further confirm the glassy state with a cooling field of H~0.1 T [Figure 6.A.6a]. Another experimental realization of slow spin relaxation in the SG or CG state can be found in the "time (t) evolution of remanent magnetization m(t) (TRM)" below $T_f$. The measurement was carried out following the field cooled (FC) protocol. The sample was cooled with a field of H=100 Oe down to 25 K from room temperature and then allowed for a waiting time tw = $10^2$ s with field applied. After the waiting time, the TRM data was recorded as a function of time for $10^4$ s after switching off the magnetic field. The TRM data can be analyzed using KWW (Kohlrausch Williams Watt) stretched exponential equation as given below

$$\mathbf{m(t)} = \boldsymbol{m_0} - \boldsymbol{m_g exp}\left\{-\left(\frac{t}{\tau}\right)^{\beta}\right\} \qquad \textbf{(6.A.5)}$$

Here, $m_0$ is the initial remanent magnetization, $m_g$ represents the magnetization of the glassy component, τ is the characteristic relaxation time constant, and β is the stretching exponent. The KWW fitting is a powerful technique which is widely used for the investigations of the m(t) data for glassy or disordered systems. The value of β covers the

dynamics of spins with very strong (β=1) to no relaxation (β=0) limit and depends on the nature of the energy barriers involved in the relaxation. For systems with a distribution of energy barriers, β lies between 0 and 1, whereas for a uniform energy barrier, β = 1. The obtained $\beta$ value for SFTS is ~ 0.58, thus confirming the existence of a glassy state at this temperature (25 K) similar to other reports on glassy system [282], [324]–[327]. This value also signifies that the system evolves through a number of intermediate metastable states, i.e., activation takes place against multiple anisotropic barriers similar to [324]. The initial rapid down fall of the m(t) data can be presumably attributed to the existence of interacting FM clusters [328]. In Figure 6.A.6b, the powder XRD pattern of $Sb_{1.9}Fe_{0.1}S_{0.15}Te_{2.85}$ is manifested.

To further explore the glassy behaviour in this system, ac susceptibility data were obtained at dc fields of various amplitudes (not shown). The $\chi''$ peak shows a decreasing trend in magnitude with increasing DC field for both Tf1 and Tf2. With increasing Hdc, the peak temperature (Tf ) moves towards low temperatures, further supporting the SG transition.

Introducing magnetic atoms may or may not cause a gap for surface Dirac electrons depending on the nature of Ruderman-Kittel-Kasuya-Yosida (RKKY) interaction. In diluted magnetic semiconductors (DMS) the most possible exchange interaction is carrier induced indirect coupling due lower concentration of magnetic impurities compared to the host atoms. The RKKY interaction describes the indirect exchange coupling between magnetic impurities mediated by the itinerant electrons and plays a vital role in topological phase transitions. Moreover, RKKY interaction has an oscillatory dependence on the distance between the magnetic moments amd become FM to AFM depending upon the distance between doped magnetic impurities. Thus, it is natural to expect that there is a close relation between the RKKY interaction and phase transition. Interestingly, all signatures provided by RKKY interaction originate from the bulk band and thus one can

probe the topological phases only by measuring the bulk states, not caring for the formation of topological states. This interaction consists of, Heisenberg-like, Ising-like and Dzyaloshinskii-Moriya (DM)terms, and are expected to be crucial game-changer behind the frustrated spin dynamics.

However, we can observe [Figure 6.A.3a] a sudden upturn in M-T data (taken under 100 Oe) near 120K for the composition $Bi_{1.9}Fe_{0.1}Te_3$, indicates random magnetic interactions are at work. Similar type of observation was reported in 2.5% Fe intercalated $Bi_2Te_3$ single crystal sample [31], quantum Griffith phase was confirmed from the power law $M \sim T^{-\alpha}$. We found $\alpha \approx 0.039$ and 1.14 before and after the cusp [Figure 6.A.3b]. The divergent behaviors and change in slope at the lower temperature imply that magnetic correlations evolve from quantum Griffiths behaviors to ferromagnetic-cluster glassy structure. A clear downward deviation from C-W fit represents the finger prints of Griffith singularity and distinguishes it from smeared phase transitions. GP is basically characterized by two features one is the presence of ferromagnetically correlated clusters and the other is absence of spontaneous magnetization in the PM region[thesis]. For the GP, on the other hand, the downturn behavior of $\chi^{-1}$ can be suppressed with the external field increasing due to polarization of spins outside the clusters [32-34]. The ordering temperature is above 350K for the two compositions Fe-S doped $Sb_2Te_3$ and $Bi_2Te_3$.

**6.A.2.5 Temperature dependent Raman** Figure 6.A.4a shows the temperature-dependent Raman spectra for the current sample in the 100-300K range. Figure 6.A.4b demonstrates contour plot of the temperature vs Raman shift, the colour variation manifests the intensity variation with temperature. At room temperature, we have identified the 3 Raman modes at $A_{1g}^1$~69.46 $cm^{-1}$, $E_g^1$~110.2 $cm^{-1}$, and $E_g^2$~168 $cm^{-1}$ along with an IR mode at $A_{2u}^2$~123.9$cm^{-1}$. These Raman modes are in good agreement with earlier reported works

on bulk $Sb_2Te_3$[207] as well as few other quintuples[107], [185], [186]. We could not observe $E_{1g}$ mode (40 $cm^{-1}$) due to the spectral width of filter[185]. The odd-parity IR active phonon modes are Raman forbidden and do not appear in the Raman spectrum for bulk crystals with crystal symmetry. Those IR-active modes also appear as Raman mode in pristine $Bi_2Te_3$ and its derivatives [229]–[231], [237]as a result of crystal symmetry breaking. Similar IR-active vibrational modes appear as Raman mode by the In-diffused $Bi_2Se_3$ and in pristine $Bi_2Se_3$[233], [329]. This particular mode appears possibly because of spin fluctuation occurring at 120K. It gets disappeared below this particular temperature and we can observe only those Raman modes as expected in rhombohedral R-3m structure. This vibrational mode reappears above 200K and continues up to room temperature because of the large thermal fluctuation. Moreover, another mode at $A_{2u}^3$~141 $cm^{-1}$ seem to arise at 200K because of the same reason and carries forward up to room temperature. As identified the variation of $E_g^2$ mode in Figure 6.A.4c, it does not indicate any structural transition down to 100K. Similar pattern is followed by M1 mode as indicated in Figure 6.A.4d.

**6.A.2.6 dHvA oscillation** For the de Haas–van Alphen (dHvA) oscillation study, we performed the magnetization measurement on the $Sb_{1.9}Fe_{0.1}S_{0.15}Te_{2.85}$ single crystals with magnetic field along the c axis. The field dependence of the magnetization data shows a hysteresis behaviour with prominent dHvA oscillation at 2K and 5K. We subtract a smooth background from the magnetization data to extract the oscillatory component $\Delta M$, and plot the result as a function of 1/B in Figure 6.A.7a. We performed the fast Fourier transforms (FFT) of M oscillation as shown in Figure 6.A.7b, which corresponds to multiple Fermi pockets. The multiple frequencies observed from the FFT spectra are $F_\alpha$~40T, $F_\gamma$~60T, $2F_\alpha$= 80T, $2F_\beta$~100T and $3F_\beta$~150T. The Pristine $Sb_2Te_3$ has a single peak at 50 T, heralding the existence of a single pocket near the Fermi surface as indicated in[111], [330].

The observed frequencies at ~62 T and ~150 T are previously observed in Fe doped $Sb_2Te_3$ due to complex fermiology[111]. We have done the inverse FFT for these two frequencies as shown in Figure 6.A.7c and d. According to Onsager's relation the oscillations frequency F is related to the cross-section area A of the Fermi surface $F = (\hbar/2\pi e) A$; where $\hbar$ is reduced is Plank's constant and e is the electronic charge. We evaluated the Fermi surface area 0.62 and 1.47 $nm^{-2}$ perpendicular to the ab plane. The Berry phase associated with charge carrier can provide further information regarding the topological character of the band structure. The Berry phase is zero for parabolic band dispersion, whereas a nontrivial Berry phase is obtained for linearly dispersed bands. For 2D and 3D band topologies, respectively, an additional phase contribution arises with values of 0 and ±1/8. The Berry phase can be

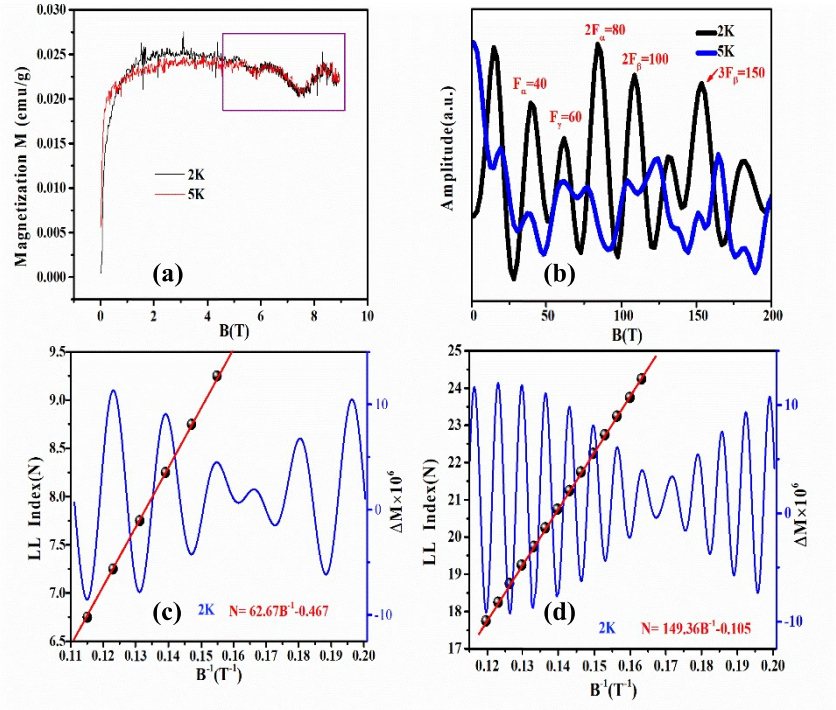


**Figure 6.A.7 (a)** dHvA oscillation in the M-H data at low temperature and high magnetic field, **(b)** FFT amplitude data on frequency scale at 2K & 5K, 5 frequencies $F_\alpha$~40T, $F_\gamma$~60T, 2 $F_\alpha$~80, 2$F_\beta$~100T, 3$F_\beta$~150T indicating Fermi surfaces of the sample, inverse-FFT with the **(c)** 60T and **(d)** ~150T data by using band- pass filter, Landau Fan diagram to obtain the frequency and phase.

calculated using the intercept of a Landau level fan diagram plotted from the quantum oscillation's extreme points. Assigning the peak position of ΔM as integer + 1/4 and valley positions as a half integer + 1/4, the intercept extracted to be 0.5 for nontrivial and 0 for trivial bandstructure. We achieved the intercept ~0.467 close to the nontrivial value (massless relativistic Fermions) for the 50T frequency.

**6.A.2.7 ARPES** Figure 6.A.8a-c displays the Angle-resolved photoemission spectrum dispersions of the present sample measured above and below the FM-AFM phase transition using 95 eV synchrotron source. ARPES obtained at 20K, 190K and 260K, demonstrating p-type behaviour and that the Fermi level, $E_F$, is near to the Dirac point. Out results are matching well with the obtained electronic band dispersion in Mn-doped $Sb_2Te_3$ at 38K[331]. On heating from 2K to room temperature, the BVB gets closer from the Fermi level. dHvA oscillation also suggests that the nontrivial topology is retained in this doped material.

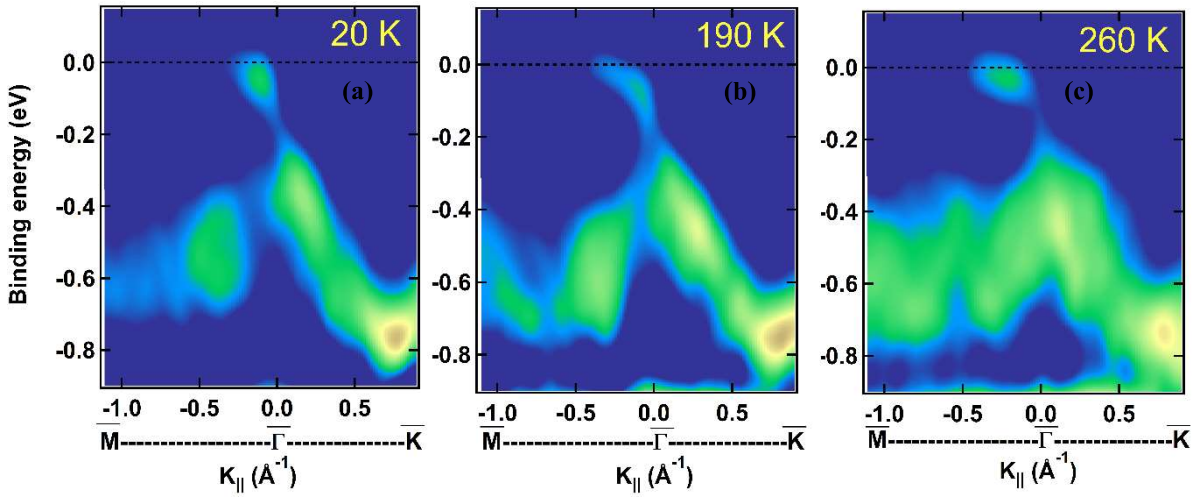


**Figure 6.A.8** Temperature dependent angle resolved photoemission spectra taken at (a) 20K, (b) 150K, and (c) 260K with Synchrotron source of 95eV.

## *B. Unusual Double Glassy phase and Anomalous Hall effect in S-doped $(BiFe)_2Te_3$ Topological Insulator*

### 6.B.1 Results and Discussions

**6.B.1.1 XRD** Figure 6.B.1a represents the single crystal XRD pattern of the $Bi_{1.9}Fe_{0.1}S_{0.15}Te_{2.85}$. Figure 6.B.4a-c presents powder XRD pattern of $Sb_{1.9}Fe_{0.1}Te_{2.85}S_{0.15}$ and single crystal as well as powder XRD pattern of $Bi_{1.9}Fe_{0.1}Te_{2.85}$.

**6.B.1.2 Resistivity behaviour** The resistivity data in Figure 6.B.2b is showing metallic behaviour below room tepmerature. The highest field (7T) MR% is 653% at 2K and reduces to 22% at 200K for this sample. The value is quite high amongst the group of materials. The Hall data in Figure 6.B.1c showing p-type characteristics or the hole dominating carrirs all the temperature range. The Hall data is not linear as clear from the behaviour and the linear part was substracted to get the behaviour obtained in Figure 6.B.1d. The extracted density and mobility are plotted as a function of temperature in Figure 6.B.1e.

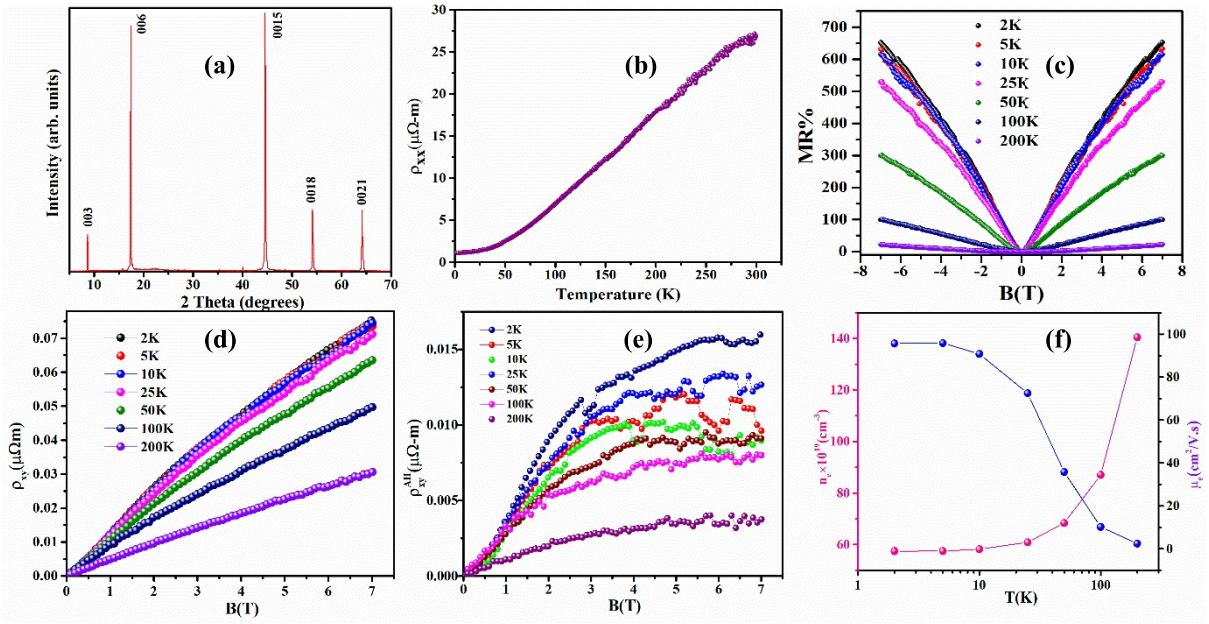


**Figure 6.B.1 (a)** Single crystal XRD pattern, **(b)**resistivity evolution with temperature at zero magnetic field, **(c)**MR% at 2K, 5K, 10K, 25KK, 50K, 100K, 200K for B⊥I configuration, **(d)** Hall resistivity at 2K, 10K, 25K, 50K,100K and 200K, **(e)** AHE effect at 2K, 10K, 25K, 50K 100K and 200K, **(f)** density and mobility evolution with temperature for $Bi_{1.9}Fe_{0.1}S_{0.15}Te_{2.85}$.

**6.B.1.3 Magnetic behaviour** We can observe a sudden upturn in M-T data (taken at 100 Oe) at about 110K for the composition $Bi_{1.9}Fe_{0.1}Te_3$, indicating random magnetic interactions are at work. The magnetization gets saturates at 120K and then starts decreasing. The Similar type of observation was reported in 2.5% Fe intercalated $Bi_2Te_3$ single crystal sample[301]; a unique quantum Griffith phase was confirmed from the power law $M \sim T^{-\alpha}$. In the present case, we found $\alpha \approx 0.040$ and 1.19 before and after the cusp. The divergent behaviors and change in slope at the lower temperature imply that magnetic correlations evolve from quantum Griffiths behaviors to ferromagnetic cluster glassy structure. The G.P signifies the presence of different sized clusters in the ferromagnetic region. At low temperature the log M-log T curve gets saturated as the cluster glasses become frozen. A clear downward deviation from C-W fit represents the finger prints of Griffith singularity and distinguishes it from smeared phase transitions. GP is basically characterized by two features one is the presence of ferromagnetically correlated clusters and the other is absence of spontaneous magnetization in the PM region[thesis]. For the GP, on the other hand, the downturn behavior of $\chi^{-1}$ can be suppressed with the increasing external field due to polarization of spins outside the clusters[332]–[334]. Figure 3 shows $log_{10}\chi^{-1}$ vs T plots at different applied magnetic fields of 100 Oe and 1000 Oe. One can observe that the downturn is markedly get softened under the high magnetic field, which supports the presence of the GP in this sample. The similar phenomena is not observed upto 350K as the PM transition temperature is comparatively higher for the case S doped BTFdc magnetization studies of BFST and BFT.

The temperature dependence of dc magnetization M(T) of BTFS measured under 100 Oe and 1000 Oe using ZFC FC protocol. Fig 7(a). shows a peak near $T_{G1}$=4K, $T_{G2}$=31K and $T_m$=110K in agreement with the reports on $Sb_{1.9}Fe_{0.1}S_{0.15}Te_{2.85}$.

The freezing temperatures $T_{G1}$ and $T_{G2}$ shift to lower temperature and magnetization increases on highering the field from 100 Oe to 1000 Oe. The shifting of $T_G$ to lower temperatures with increasing magnetic field, signature of the frozen state which gradually destroy under large magnetic fields. This is common among many SG/CG systems [305], [335], [336].The ZFC and FC magnetization curves start to separate from each other at an irreversibility temperature above $T_{irr}$=300 K and they begin to diverge strongly at low temperatures, also the freezing temperature is far away from irreversible temperature which

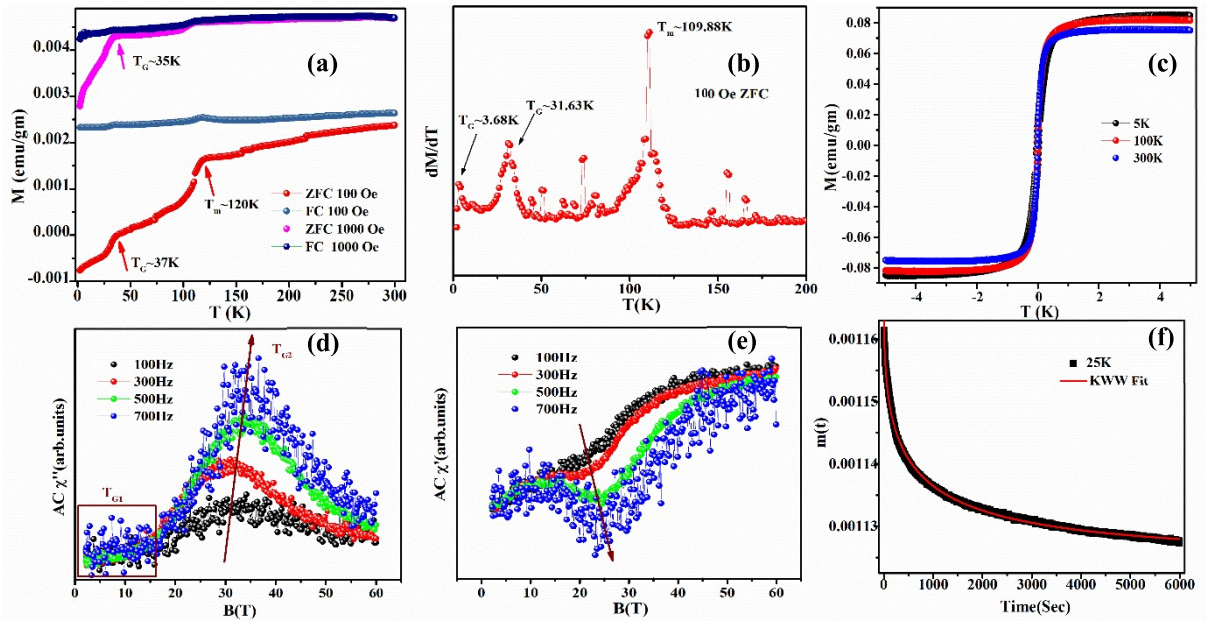


**Figure 6.B.2 (a)**Temperature dependent dc magnetization M(T) measured at different applied fields (100 Oe and 0.1T) for ZFC and FC protocols, **(b)** dM/dT as a function of temperature, **(c)** Magnetization as a function of external magnetic field at T=5 K, 100K and 300K **(d)** real ($\chi'$) and **(e)** imaginary ($\chi''$) components of the ac susceptibility measured at frequencies varying from 100 to 700 Hz, **(f)** time dependence of thermoremanent magnetization at 25 K for 0.1T cooling field. The solid line is the best fit for KWW function to the data for $Bi_{1.9}Fe_{0.1}S_{0.15}Te_{2.85}$.

contradicts the concept of canonical SG system[337]. However, the fact that $T_G$ is far below $T_{irr}$ in present case, indicating the possibility of a cluster glass (CG) state at low temperatures[338], [339]. The ZFC curve continously increases upto 300K for 100 Oe field whereas 1000 Oe curve started saturating above 150K. This increasing trend in

magnetization from ZFC M(T ) response is of a typical AFM type. The maxima of the curve found on plotting dM/dT curve as a function of temperature. The M-H curve in Fig6. (b) shows negligible hysteresis at low temperature and the magnetization saturates above 2T. This is another clarirification for the system to be a antiferromagnetic dominating behaviour. The S-shaped M-H curve as well as the glassy behaviour at low temperature can result from random FM and AFM spin correlation through intermediate complecated spin dynamics. Again the presence of MI-MI exchange interactions gives rise to the formation of magnetic clusters with different sizes in the entire system[302].

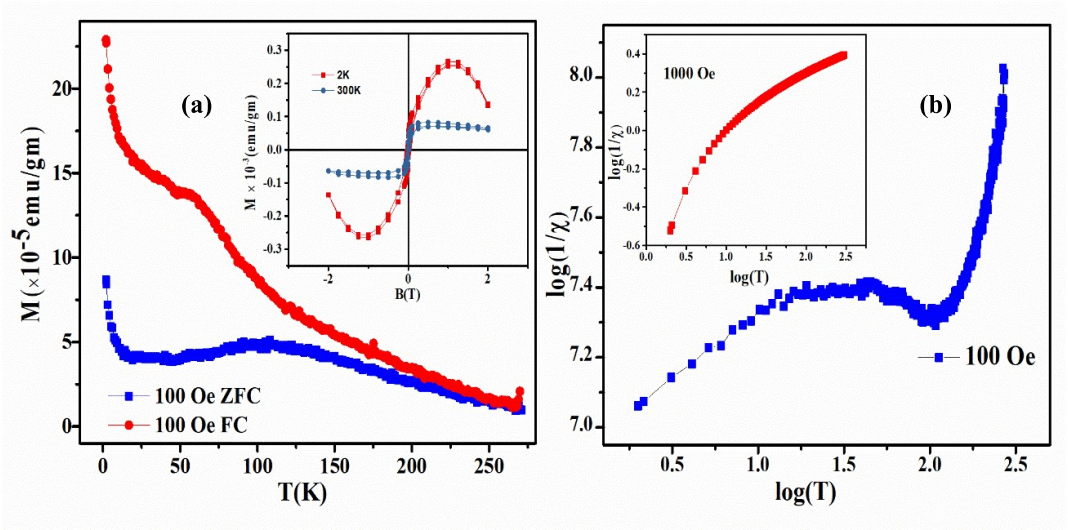


**Figure 6.B.3** (a) DC Magnetization measured in ZFC and FC protocol taken at 100 Oe. **Inset:** M(H) at 2K and 300K (b)The log-log plot of the $\chi_{dc}^{-1}$ vs temperature at 100Oe, Inset shows the suppression of GP at higher field(1000 Oe) for $Bi_{1.9}Fe_{0.1}Te_3$.

Temperature evolution of magnetic moment in Fe doped Bi2Te3 shows an irreversibility between ZFC-FC data in Fig.8 (a). Sudden increase in magnetic moment (M vs T) near 120K and a change in average magnetic interation (FM to AFM) at this temperature is consistent with[301]. The AFM nature was clarified by fitting the data with Curie-Weiss formula, a negative $\theta_{CW}$ above 150K is confirmation of the above argument. The M-H characteristic curve at 2K and 300 K reveals weakly ferromagnetic behavior with

diamagnetic background [see inset of Figure 6.B.3a] in contrast to paramagnetic phase [302] with diamagnetic background in Fe doped (x=0-0.3) $Fe_xBi_{2-x}Te_3$, although our data is similar to [305] with x=0-0.08. Quantum Griffith phase like bahaviour is evident below paramagnetic state from the log(1/χ) vs logT plot. This can be proved by fitting the data with a power law $\chi^{-1} \alpha T^{1-\lambda}$ ; λ=0 near 112K and 1 near 210K which is a paramagnetic regime. It gets saturated near 30K indicating ferromagmagnetic clusters become frozen at this temperature. One can see that the downturn is markedly suppressed (inset of Figure 6.B.3b) under the high magnetic field (1000 Oe), which is the hallmark of presence of the GP in this sample. This softening in downturn is due to the increasing paramagnetism with field and dominates over the FM cluseters. Griffiths phase is actually the appearance of finite-size ferromagnetic clusters in paramagnetic phases where the spins are ferromagnetically correlated within the clusters. However, the system as a whole would not develop any long range ordering and thus no spontaneous magnetization would appear. However for BFST sample we can not observe such GP in the system, indication towards LRO. Importantly M-T data at 100 Oe data has strong irriversibility below 200K whereas higher field (1000 Oe) data has reduced bifucation due to the usual destruction of glassy behaviour with increasing DC field.

**6.B.1.4 ac susceptibility study** The measurements were performed at an ac field of $H_{ac}$ = 3.5 Oe and at various frequencies ranging from 100–700 Hz. Figure 6.B.2d and e shows the temperature dependence of the real (χ′) and imaginary (χ″) components of the ac susceptibilitydata for BFST. χ″(T ) data obtained at 100 Hz exhibit a broad peak near 30 K and shifts towards higher temperature as the frequescy reches to 700Hz. The frequency shift near ~4K is not sharp compared to the 30K. Both the peaks are consistent with DC magnetization data and obeserved to shift towards higher temperature with increasing frequency. With increasing frequency the magnitude of the peaks incease significantly. The

$\chi''(T)$ data [Fig. 9(a)] exhibits similar behavior with the exception that the frequency dependence of the data for both the peaks are more significant when compared to the $\chi'(T)$ data. The frequency dependence of the ac susceptibility and the observations of those peaks below ordering temerature in the this system shows cluster glass, or RSG state, exists within the material. However this type of transion is in common for CG/SG/SPM blocking. So for the further verification we go for calculating Mydosh parameter (**Equation 6.A.1**). The p value is 0.089 for $T_G$ and in the range of cluster glass. Moreover, in an SG or CG state, the spin dynamics gets slowed down below the critical temperatures $T_G$. This critical slowing down of spins near $T_G$ can be investigated using the dynamic scaling law Fig.10 (a), (b). The best fitting (**Equation 6.A.2**) of the "f vs $T_f$" curve by Dynamic scaling yielded~ $\tau_0=8.12\times10^{-5}$s, $T_{SG}$= 18.289K, and, $z\nu=3.083$. For further investigations of inter-cluster interactions, the empirical Vogel-Fulcher (VF) law (**Equation 6.A.3**) was employed to fit the above curve "f vs $T_f$" shown in Fiure 6.B.3 a, b. The obtained fitting values are ~ $E_A$=2.88meV, $T_0$= 15.970K as obtained. $T_0$ is also considered as a qualitative measure of the intercluster interaction strength in the system. A nonzero value of $T_0$ arises from the interaction between the spins and indicates the formation of spin clusters. The $\tau_0$ value obtained from the Vogel–Fulcher fitting for $T_{f2}$ is $4.35\times10^{-5}$s. Further, the fact that $T_0$ is very close to Tf suggests that the Ruderman-Kittel-Kasuya-Yosida (RKKY) interaction is relatively strong in our compound[283]. Moreover the Tholence criterion[45]n gives the 0.23 (**Equation 6.A.4** )when $T_f$ is 20.65K, taken at smallest excitation frequency, this value is comparable to the systems with progressive freezing[286].

**Table 6.B.1** Parameters obtained from the Dynamic fitting analysis using Eqs. (5) for $T_{G2}$

| $T_f$(K) | $\tau_0$ (s) | $T_{SG}$(K) | zv |
|---|---|---|---|
| 22K | $8.109\times10^{-5}$ | 18.289±1.679 | 3.08 ±0.77 |

**Table 6.B.2** Parameters obtained from the V-F fitting analysis using Eqs. (6) for $T_{G2}$

| $T_f$(K) | $\tau_0$ (s) | $T_0$ (K) | $E_A/K_B$ (K) |
|---|---|---|---|
| 22K | 4.35×10 | 15.970±2.749 | 33.5169 |

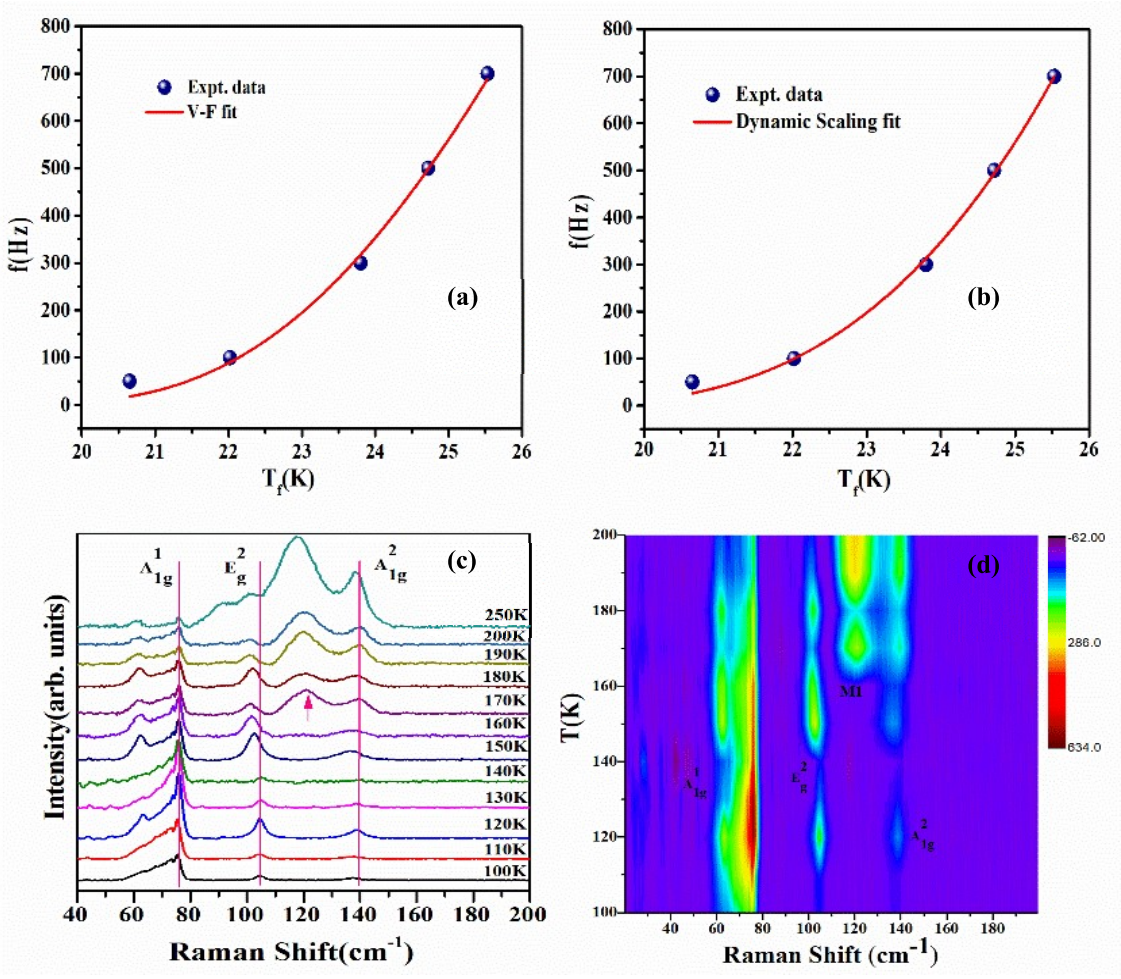


**Figure 6.B.4** Dynamic scaling (a), (b) and Vogel-Fulcher (c), (d) fits of the "Tf vs f" curve respectively for $T_{f1}$ and $T_{f2}$ of $Bi_{1.9}Fe_{0.1}S_{0.15}Te_{2.85}$.

To further explore the glassy behavior, ac susceptibility data were obtained at different dc magnetic fields (not shown). The ac susceptibility data performed as a function of temperature at various ac fields and a frequency of 157 Hz. For both the $\chi'(T)$ and $\chi''(T)$ data, both the peaks are in decreasing in magnitude with increasing dc magnetic field. This response supports with usual magnetic system exhibiting such type of magnetic behaviour.

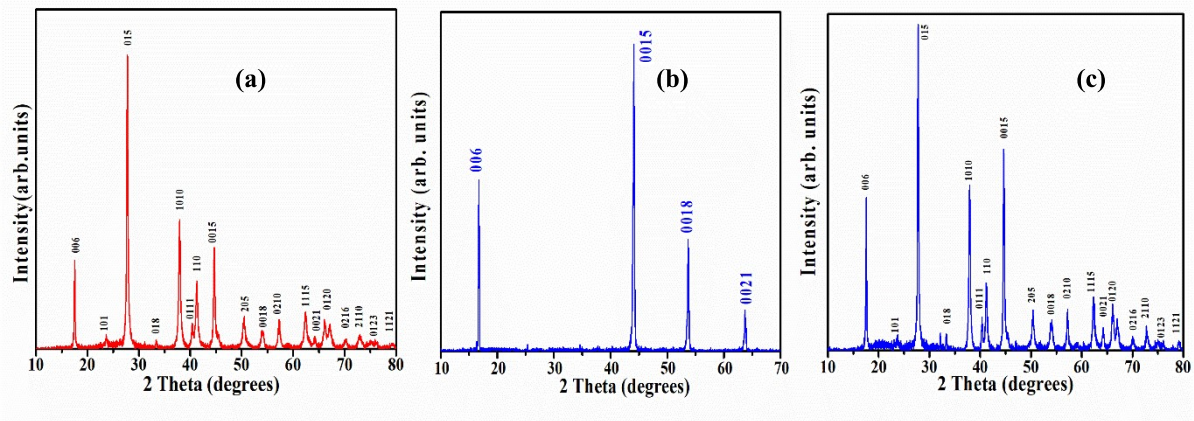


**Figure 6.B.5 (a)** Powder XRD pattern of $Bi_{1.9}Fe_{0.1}S_{0.1}5Te_{2.85}$, **(b)** single crystal XRD and **(c)** powder XRD pattern of $Bi_{1.9}Fe_{0.1}Te_{2.85}$.

The isothermal temporal relaxation of the remanent magnetization (TRM) at 25K was also performed to further confirm the glassy state similar to Fe and S doped $Sb_2Te_3$ compound. It is evident that (Figure 6.B.2f) even after such a long time of 6000s, the decay in the residual magnetization continues which is a typical aspect of disordered glassy states owing to the existence of the hierarchical arrangements of the meta-stable states[340], [341]. The KWW fitting (**Equation 6.A.5**) is a powerful technique for investigating glassy or disorderedness in the system from m(t) data and it lies between 0-1. Our attempt to fit the data with KWW model results in β value equals to 0.411, the intermediate value indicate a non-Debye behavior with distribution of relaxation times due to the presence of a large number of degenerate states in the frozen state thus confirming the existence of a glassy

state at this temperature (25 K). The initial rapid down fall of the m(t) data can be presumably attributed to the existence of interacting FM clusters[328].

On the basis of the above discussion, we argue that the long-range ordering coexists with the FM cluster glass state in Fe and S doped Bi2Te3 at low temperature due to competitive FM and AFM correlation in the system. However the presence of GP in Fe doped $Bi_2Te_3$ is confirmation of absence of such LRO. We captured the significant changes between S doped $Bi_{1.9}F_{0.1}Te_3$ and without S doped -$Bi_{1.9}F_{0.1}Te_3$ system. The substitution of S introduces makes the system to host both metastable states and Dirac quasiparticles. We also found that Fe impurities tend to aggregate to form FM-ordered clusters at low temperature. The complex spin dynamics and competition between FM and AFM correlation is the precursor for the CG state in the Fe and S doped system. The Fe doping x=0.1 in Bi2Te3 provokes considerable Fe-Fe exchange interaction along with the formation of a no of clusters with different sizes. The clusters' mean size and the number of clusters depend on temperature; they increase by increasing temperature, pass through a maximum at a critical temperature, and decrease toward zero at high temperatures according to the report of [340], [341].

**6.B.1.5 Temperature dependent Raman** Figure 6.B.3a shows the temperature-dependent Raman spectra for the current sample in the 100-300K range. Figure 6.B.3b demonstrates contour plot of the temperature vs Raman shift, the colour variation manifests the intensity variation with temperature. The inter-planer force for the corresponding modes determines the frequency of the vibrational modes. All vibrational modes are solely Raman active or infrared (IR) active because to inversion symmetry. 15 different vibrational patterns can be produced using the R-3m symmetry, out of which of 3 are acoustic modes and 12 are optical modes, respectively. The group theory states that 4 of the 12 optical modes are $2A_{1g}$ and $2E_g$ are Raman active while the remaining eight are IR active. Transverse optical mode

(TO) are the Raman active $E_g$ modes that vibrates in the plane of the crystal. The longitudinal optical modes (LO) that oscillate perpendicular the the plane of the crystal are $A_{1g}$ modes. At room temperature, we can identify the 3 Raman modes at $A_{1g}^1$~61 $cm^{-1}$, $E_g^1$~100.8 $cm^{-1}$, and $E_g^2$~138.4 $cm^{-1}$ along with an IR mode at $A_{1u}$~117.86$cm^{-1}$. These Raman modes are in good agreement with earlier reported works on bulk $Bi_2Te_3$[229]. We could not observe $E_{1g}$ mode (40 $cm^{-1}$) due to the spectral width of filter[185]. The odd-parity IR active phonon modes are Raman forbidden and do not appear in the Raman spectrum for bulk crystals with crystal symmetry. Those IR-active modes also appear as Raman mode in pristine $Bi_2Te_3$ and its derivatives [229]–[231], [237] as a result of crystal symmetry breaking. This particular mode appears possibly because of thermal fluctuation as a consequence of excess of charge carriers at higher temperature. So the crystal symmetry breaks. This particular mode disappears at low temperature and we can observe only those Raman modes as expected in rhombohedral R-3m structure. This vibrational mode appears only above 160K and continues up to room temperature.

We have presented evidence for two cluster glass transitions in the $Sb_{1.9}Fe_{0.1}S_{0.15}Te_{2.85}$ and its sister compound $Bi_{1.9}Fe_{0.1}S_{0.15}Te_{2.85}$ system using a series of bulk measurements revealing history dependent effect, critical slowing down of the spin dynamics and stretched exponential decay of the thermoremanent magnetization. Analysis of the ac susceptibility measurements reveals power-law/Vogel-Fulcher-type critical spin dynamics with a time scale of $\tau 0 \sim 10^{-6}$ s, $10^{-5}$ s suggests the existence of two cluster spin glass phases at 4K and 30K in both the system. The observation of slow relaxation of thermoremanent magnetization taken below the SG transition temperature supports glassy phase near $T_{SG}$~30K. We notice that addition of S can provide a unique platform for direct observation of a no of glassy phases via a study of dynamical susceptibility at the spin-glass transition temperatures (TSG).

**6.B.1.6 ARPES study** Figure 6.B.5a-c displays the Angle-resolved photoemission spectrum dispersions of the present sample measured above and below the FM-AFM phase transition using 95 eV synchrotron source. ARPES obtained at 20K, 190K and 260K, demonstrating p-type behaviour and that the Fermi level, $E_F$, is near to the Dirac point. As the temperature increases, Fermi level is coming upwards whereas Dirac point is going downwards indicating p-type behaviour.

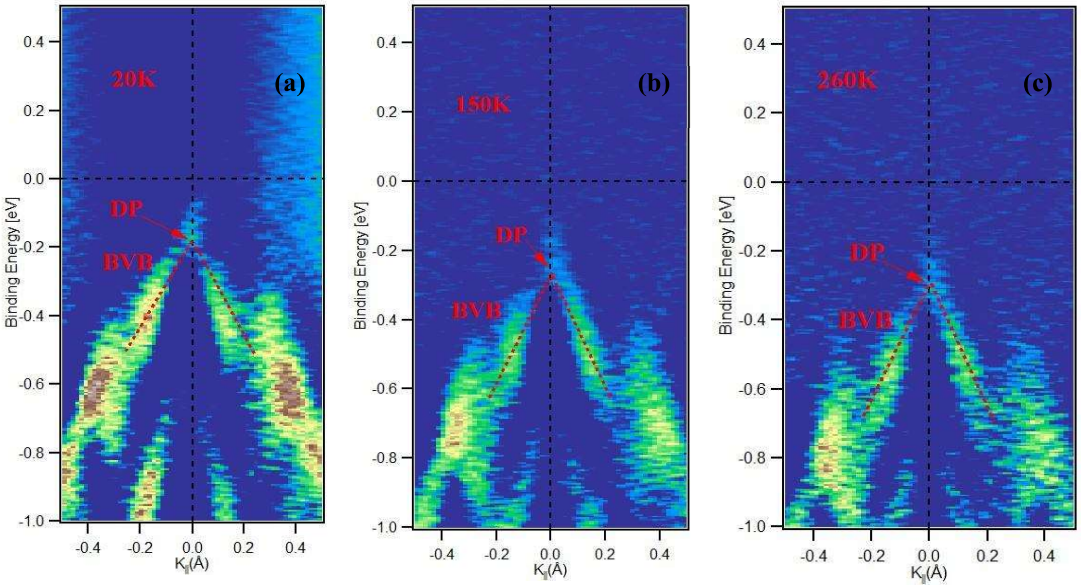


**Figure 6.B.6** Temperature dependent angle resolved photoemission spectra taken at (a) 20K, (b) 150K, and (c) 260K with Synchrotron source of 95eV.

## 6.B.2 Conclusions

Due to fundamental and technological concerns, investigating materials with topological magnetic structures has always been a focus of significant research. We explored $Sb_{1.9}Fe_{0.1}Te_{2.85}S_{0.15}$ and $Bi_{1.9}Fe_{0.1}Te_{2.85}S_{0.15}$ where multiple magnetic phases - a unique combination of disordered glassy phase, competitive FM-AFM interactions and nontrivial surface state coexisted at the same time, we also observed a Griffith phase at low temperature when we added only Fe into $Sb_2Te_3$ or $Bi_2Te_3$. We have discussed the impact of those complicated magnetic phases upon the observed AHE in $Sb_{1.9}Fe_{0.1}Te_{2.85}S_{0.15}$ and

$Bi_{1.9}Fe_{0.1}Te_{2.85}S_{0.15}$ with magnetotransport studies. The ac-susceptibility results demonstrate a shift in the freezing temperature with excitation frequency, the comprehensive analysis verifies the slower dynamics and a non-zero Vogel-Fulcher temperature $T_0$ suggests cluster spin glass. This, together with an intermediate value of the Mydosh parameter provides an evidence for the formation of a cluster glass state in the present system. Topological frustrated magnets, which can host both magnetic fluctuations and Dirac quasiparticles, are highly sought after class of compounds. Furthermore, as seen by the de Haas-van Alphen (dHvA) oscillation study, the fermiology deviates with doping and produces multiple Fermi pockets, revealing a rich complexity in the underlying electronic structure for the $Sb_{1.9}Fe_{0.1}Te_{2.85}S_{0.15}$. From the temperature dependent Raman data we cannot see any structural transitions to exist in the temperature range 100-300K. This work gives exiting direction to study topological magnetic structure in various materials.